FRONTIERS OF PHYSICS

RESEARCH ARTICLE
Volume 17 / Issue 3 / 33506 / 2022

The reservoir learning power across quantum many-body localization transition

Wei Xia[1], Jie Zou[1], Xingze Qiu[1,2,†], Xiaopeng Li[1,3,‡]

1 State Key Laboratory of Surface Physics, Institute of Nanoelectronics and Quantum Computing, and Department of Physics, Fudan University, Shanghai 200433, China
2 Shenzhen Institute for Quantum Science and Engineering, Southern University of Science and Technology, Shenzhen 518055, China
3 Shanghai Qi Zhi Institute, AI Tower, Xuhui District, Shanghai 200232, China
Corresponding authors. E-mail: †xingze@fudan.edu.cn, ‡xiaopeng_li@fudan.edu.cn
Received February 15, 2022; accepted March 1, 2022

ABSTRACT

Harnessing the quantum computation power of the present noisy-intermediate-size-quantum devices has received tremendous interest in the last few years. Here we study the learning power of a one-dimensional long-range randomly-coupled quantum spin chain, within the framework of reservoir computing. In time sequence learning tasks, we find the system in the quantum many-body localized (MBL) phase holds long-term memory, which can be attributed to the emergent local integrals of motion. On the other hand, MBL phase does not provide sufficient nonlinearity in learning highly-nonlinear time sequences, which we show in a parity check task. This is reversed in the quantum ergodic phase, which provides sufficient nonlinearity but compromises memory capacity. In a complex learning task of Mackey–Glass prediction that requires both sufficient memory capacity and nonlinearity, we find optimal learning performance near the MBL-to-ergodic transition. This leads to a guiding principle of quantum reservoir engineering at the edge of quantum ergodicity reaching optimal learning power for generic complex reservoir learning tasks. Our theoretical finding can be tested with near-term NISQ quantum devices.

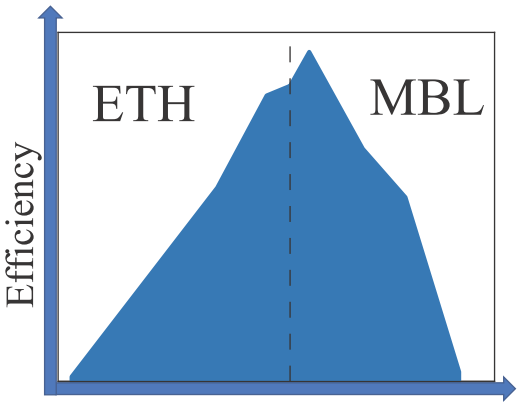

Keywords quantum reservoir computing, many-body localization, quantum ergodic, edge of quantum ergodicity, optimal learning power

1 Introduction

Recent experimental demonstration of the fascinating quantum computation advantage with superconducting qubits [1] and interfering photons [2] has triggered monumental research interests in applications of quantum computing. Although a scalable error-corrected quantum computer is still unavailable, a large degree of controllability has been available in a broad spectrum of noise-intermediate-scale quantum (NISQ) devices [3–5], including atomic [6], photonic [7, 8], and solid-state systems [9, 10], whose numerical simulations are exponentially costly in classical computation resources. This suggests compelling quantum computational power embedded in the present NISQ devices, of potential importance to applications in science discovery [11], cryptography [12], and optimization [13]. How to harness the quantum computational power and how the computational power manifests in the present NISQ devices demand theoretical investigation. This is particularly crucial for quantum systems lacking full programmability.

For classical systems, one way to characterize their com-

Higher Education Press

arXiv: 2104.02727
https://doi.org/10.1007/s11467-022-1158-1

putational power is from the learning capability within the framework of reservoir computing [14], where the system is interfered by manipulating the input and output only with the system itself untouched as a "black box". In time sequence learning, it has been found that the complex dynamics in the "black box" mediates both memory and nonlinearity in mapping the input to the output. It has been demonstrated that a classical dynamical system at the phase edge of a chaotic region [15–19] develops optimal learning power as it maintains a balance between integrability and chaoticity that nurture long-term memory and complex nonlinearity.

Generalizing the concept of reservoir computing to quantum dynamical systems leads to quantum reservoir computing (QRC) [20–24], that does not require precise or full quantum control of the quantum system. This approach provides a plausible route to harness the ultimate quantum computation power of NISQ devices [25]. However, what quantum systems would exhibit optimal learning power in reservoir computing remains to be understood.

In this work, we study the learning power of a one-dimensional quantum reservoir composed of long-range randomly-coupled qubits (Fig. 1). This system has a quantum many-body localization (MBL) transition with varying the disorder strength. We investigate the learning performance on two computation tasks of Boolean function emulation including the short-term memory (STM), and the parity check (PC) tasks, which characterize the memory capacity and the amount of nonlinearity of the quantum reservoir, respectively [20]. In the MBL phase, learning the STM task outperforms the PC task significantly, which we attribute to the extensive number of emergent local integrals of motion in the MBL phase [26–29]. In the quantum ergodic phase [30], we find the opposite, which implies the quantum dynamics in the ergodic phase mediates larger amount of nonlinearity, more resembling the chaotic dynamics in classical systems. We further examine the learning power of the disordered quantum many-body system on the Mackey–Glass (MG) prediction task [31], whose performance requires both memory and nonlinearity. In this task, we find that the learning power develops a peak around the quantum MBL-to-ergodic phase transition. This work would shed light on the quantum reservoir engineering to invest most quantum learning power for complex reservoir computing tasks.

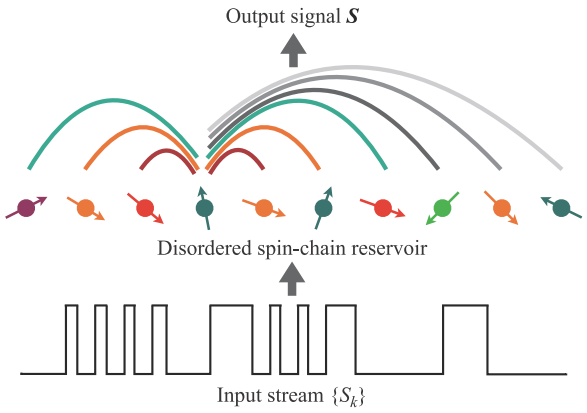

Fig. 1 Illustration of quantum reservoir computing with a disordered quantum spin chain with long-range interactions. The information from the input stream $\{s_k\}$ is fed into the reservoir for information processing. The output signal $\boldsymbol{S}$ is collected by quantum measurements on the reservoir qubits.

2 The quantum reservoir computing setup

In QRC [20], the system is initialized as an infinite temperature state at time $t = 0$. The quantum reservoir dynamics corresponds to a unitary time evolution of N qubits described by a time-dependent density operator, $\rho(t)$, sequentially interrupted by an input signal $\{s_k\}_{k=1}^{M}$, where s_k takes binary numbers 0 and 1 for a discrete signal, or values in between in a continuous setting. The time evolution is chopped into multiple τ-durations, i.e., $t = k\tau$, with each duration further split into V subintervals. At time $t = k\tau$, the time evolution is interrupted by the input as $\rho(t) \mapsto \rho(t + 0^+) = \rho_{s_k}^{[1]} \otimes \mathrm{tr}_1[\rho(t)]$, where tr_1 is a partial trace with respect to the first qubit, and the state of the first qubit is modified to $\rho_{s_k}^{[1]} \to |\psi_{s_k}\rangle\langle\psi_{s_k}|$, with $|\psi_{s_k}\rangle = \sqrt{1-s_k}\,|+\rangle + \sqrt{s_k}\,|-\rangle$, and $|\pm\rangle$, the eigenstates of the Pauli-X operator. Note that here the information is encoded with the σ_x basis rather than the σ_z basis encoding. The σ_z basis encoding which has applied to the NARMA task [20, 32], does not perform well for the complicated learning tasks presented in this work (see Appendix A). Measurements are performed in the Pauli-X basis at the end of each subinterval. The resulting output signal is denoted as $\boldsymbol{S}$, with elements $S_{k,v,i} = (1 + \mathrm{tr}[\rho(k\tau + \tau v/V)\, X_i])/2$, v and i indexing subintervals and qubits, respectively.

In learning a time-sequence defined by a nonlinear function, $y_{k'}^{\star} = f(\{s_{k\le k'}\}; k')$, we cast the time steps into three groups $\{K_1, K_2, K_3\}$, with the casted time sequence and the reservoir output signal represented by a set of vectors $\{\boldsymbol{y}_1^{\star}, \boldsymbol{y}_2^{\star}, \boldsymbol{y}_3^{\star}\}$, and matrices $\{\boldsymbol{S}_1, \boldsymbol{S}_2, \boldsymbol{S}_3\}$ accordingly. The starting time steps K_1 are discarded to remove the effect of initialization. The following time steps K_2 are used for training a linear regression model, $y_k = \sum_{v,i} S_{k,v,i} W_{v,i} + B_k$ with Ws and Bs fitting parameters introduced to minimize the Frobenius norm $\|\boldsymbol{y} - \boldsymbol{y}^{\star}\|$. The final time steps K_3 are for prediction, using the reservoir output $\boldsymbol{S}_3$ and the trained linear regression model, by which a time sequence $\boldsymbol{y}_3$ is predicted. The performance of the reservoir computing is quantified by a normalized covariance, $C = \mathrm{cov}(\boldsymbol{y}_3^{\star}, \boldsymbol{y}_3) / [\sigma(\boldsymbol{y}_3^{\star})\,\sigma(\boldsymbol{y}_3)]$, with σ the standard deviation. Its average $\overline{C}$ is obtained by sampling distinctive input-signals (s_k).

3 Disordered quantum spin chain reservoir

We consider a one-dimensional long-ranged coupled transverse-field Ising model as the quantum reservoir (Fig. 1), whose dynamics is governed by the Hamiltonian,

$$H = \sum_{1\leqslant i<j\leqslant N} J_{ij} X_i X_j + \frac{1}{2}\sum_{i=1}^{N} (B+\phi_i)\, Z_i\,. \tag{1}$$

Here, X and Z are the Pauli operators, $J_{ij} = J_0|i-j|^{-\alpha}$ represent the long-range power-law decaying Ising couplings, and the transverse field contains a background constant part B, and a random part, ϕ_i drawn from $\left(-\frac{W}{2}, \frac{W}{2}\right)$ according to a uniform distribution. Hereafter, the coupling strength J_0 is set as energy unit. In this work, we choose $B = 4$, and the main findings are largely independent of this parameter choice. This disorder spin model has a MBL to quantum ergodic transition, at a critical disorder strength $W_{\rm C}$ [33]. Long-range coupling is considered here to support sufficiently complex dynamics for QRC. To characterize the learning power, we average over the disorder samples and input signals.

The QRC model in Eq. (1) can be realized in experiments with the present NISQ devices including NMR [34], trapped ions [35, 36], and Rydberg atoms [37]. With NMR, the required Hamiltonian is realizable by pulse shaping [38, 39]. With trapped ions, the model has already been used to investigate the MBL transition [40] and discrete time crystals [41]. With Rydberg atoms, the Ising couplings take specific forms with exponents $\alpha = 3, 6$ [37, 42, 43], and generic long-range interacting models can be engineered with the quantum wiring scheme [44]. In our numerical results to present below, we neglect the backaction effects in the measurements to comply with the NMR system [34]. We also confirm the main findings still hold when the backaction is incorporated.

4 Short-term memory task

We first evaluate the memory capacity of our quantum spin-chain reservoir through STM task [20], where the targeting time-sequence function is $y_k^\star = s_{k-k_\Delta}$ with k_Δ representing the time delay. The learning performance on this linear task reflects the reservoir memory capacity. Figure 2 shows the QRC performance across the MBL transition. We find that the learning performance has a non-monotonic dependence on the time duration τ, reaching an optimum at a certain intermediate value τ_c. The increase of $\overline{C}$ at small τ is because the reservoir dynamics is essentially frozen with a too small choice of τ, and that the information injected through the first qubit is washed away by the subsequent inputs without capability of sharing and storing the information collectively in the reservoir. At $\tau > \tau_c$, the decrease of $\overline{C}$ with τ happens because the information would become more hidden in many-body correlations [45, 46], which cannot be extracted by the local measurements. An intermediate value of τ should be used in order to maximize the learning power of the reservoir. As we increase the disorder strength, the learning performance exhibits a monotonic increase, demonstrating an apparent advantage of the MBL phase ($W > W_{\rm C}$) in memory holding, compared with the quantum ergodic phase ($W < W_{\rm C}$). We attribute this to the emergence of local integrals of motion in the MBL phase [26–29]. With these conserved quantities, the information stored in the Pauli-X basis scrambles very slowly through a logarithmic dephasing process in quantum dynamics [47–49].

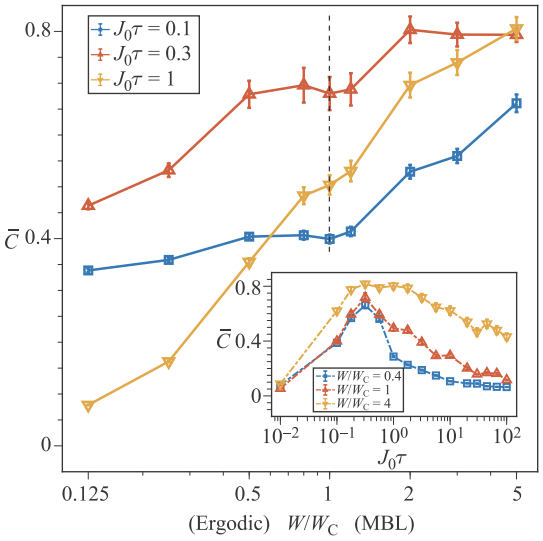

Fig. 2 The quantum reservoir learning performance on the short-term memory task with varying disorder strength. The normalized covariance $\overline{C}$ characterizes the degree of how the reservoir prediction matches the targeting time sequence. The learning performance monotonically improves with increasing disorder strength (W). This is found for a broad range of time duration τ (see the main text). The inset shows the dependence of $\overline{C}$ on τ. The reservoir is in the MBL (ergodic) phase when $W/W_{\rm C} > 1$ ($W/W_{\rm C} < 1$), with the phase boundary marked by the black "dashed" line. Each task instance consists of 5000 time steps, with the first 1000 steps discarded, the middle 3000 steps used for training, and the last 1000 steps for reservoir prediction and performance evaluation. Here, we set the qubit number $N = 10$, the number of subintervals $V = 10$, the time delay $k_\Delta = 16$, and the interaction exponent $\alpha = 0.4$. The results are averaged over 100 random samples, with the statistical error provided in the plot.

5 Parity check task

The second learning task we examine with our QRC is PC, for which the learning function is $y_k^\star = \left(\sum_{m=0}^{k_\Delta} s_{k-m}\right) \bmod 2$. This function is highly nonlinear, and the QRC learning performance then reflects the amount of nonlinearity in the reservoir. Figure 3 shows our numerical results. As the time duration τ is increased,

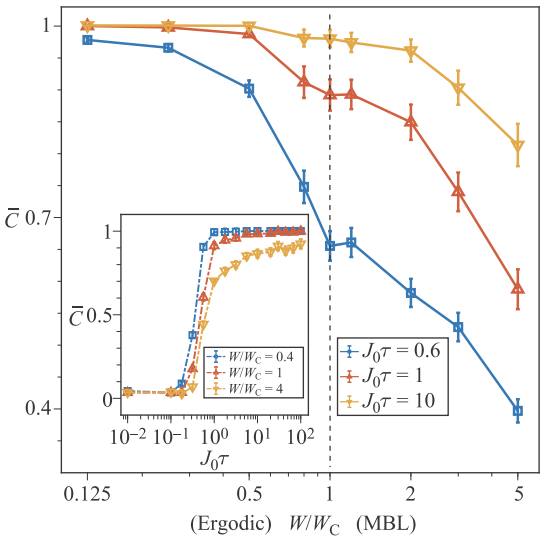

Fig. 3 The quantum reservoir learning performance on the parity check. The learning performance characterized by the normalized covariance $\overline{C}$ monotonically decreases with the disorder strength (W), as opposite to the STM task. The MBL to quantum ergodic phase transition boundary is indicated by the vertical black "dashed" line. The inset shows the dependence of $\overline{C}$ on the time duration τ, having a monotonic increasing and saturation behavior. In this plot, all parameters are chosen the same as the results of STM task in Fig. 2, except for the time delay set by $k_\Delta = 4$ here.

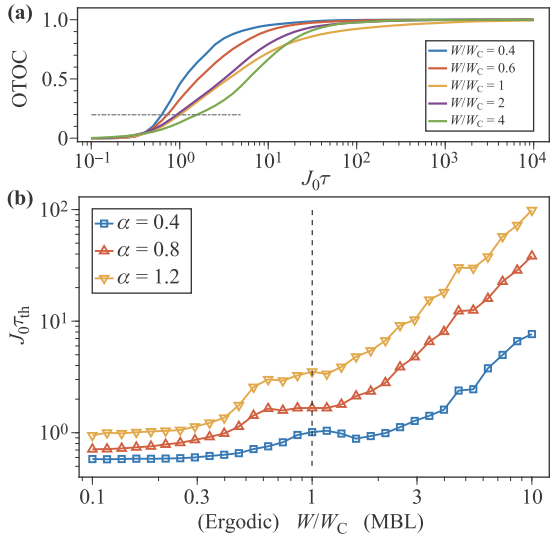

Fig. 4 Quantum information scrambling with the disordered quantum spin chain reservoir. **(a)** The averaged OTOC as a function of the time duration τ for different disorder strengths (W). The results are averaged over 100 random disorder samples. In (a), the interaction exponent is fixed at $\alpha = 0.4$. The horizontal black "dash-dotted" line marks a threshold OTOC value of 0.2 (see the main text). A time scale $\tau_{\rm th}$ is defined as the point where OTOC crosses the threshold line. **(b)** The threshold time $\tau_{\rm th}$ as a function of the disorder strength, with different α exponents. The vertical black "dashed" line indicates the MBL to quantum ergodic phase transition boundary. Here we choose a qubit number, $N = 10$.

we find that $\overline{C}$ monotonically increases, and then saturates to 1 at large τ. With increasing disorder strength for $J_0\tau \leq 1$, the learning performance becomes slightly worse within the quantum ergodic phase, and bends downward dramatically across the MBL transition — the learning power of the quantum ergodic phase thus outperforms the MBL phase for the PC task. In the quantum ergodic phase, the Heisenberg time evolution of the Pauli-X operators is strongly coupled with an exponential number $(4^N - 1)$ of all Pauli operators, which then resembles the classical chaotic dynamics, providing a larger degree of nonlinearity than the integrable MBL phase.

To gain more insight about the nonlinearity of the quantum reservoir, we look into the intrinsic chaotic properties of the quantum reservoir and calculate the out-of-time-order-correlator (OTOC) [50, 51],

$$O(\tau) = 1 - \frac{1}{N-1}\sum_{i=2}^{N}\left\langle X_1^\dagger(\tau)X_i^\dagger X_1(\tau)X_i\right\rangle , \qquad (2)$$

with $X_1(\tau) = \mathrm{e}^{\mathrm{i}H\tau}X_1\mathrm{e}^{-\mathrm{i}H\tau}$ and $\langle\cdot\rangle$ an average over a thermal ensemble at infinite temperature. The OTOC has been introduced in the literature to diagnose quantum chaos by generalizing Poisson brackets and Lyapunov exponent from classical dynamical systems [52]. Here it captures the information spreading from the first qubit to the rest. From Fig. 4(a), we see that OTOC increases monotonically with the time duration τ and then saturates, which closely correlates with the learning performance in Fig. 3. Quantum chaotic dynamics as illustrated by OTOC is beneficial for producing nonlinearity. Since all the present NISQ devices have limited quantum coherence time [3, 4], it is crucial to know the required time scale for the QRC to reach satisfactory learning performance. We thus introduce a time scale, $\tau_{\rm th}$, where OTOC exceeds a certain threshold value (set to be 0.2 here). As shown in Fig. 4(b), we find in general the information spreads much more rapidly in the quantum ergodic phase than the MBL phase. We also find the information spreads more rapidly at a smaller α, which implies larger amount of nonlinearity with longer ranged interacting models for a given amount of evolution time. More analysis about the mechanisms of the learning power for QRC in MBL and quantum ergodic phase can be found in Appendix B. Quantum reservior learning performances in the deep MBL regions are presented in Appendix C. These findings would shed light on quantum reservoir engineering for harnessing the learning power of NISQ devices on nonlinear reservoir computing tasks.

6 Mackey–Glass task

With the STM and PC tasks, we have demonstrated maximizing the memory capacity and nonlinearity favors the

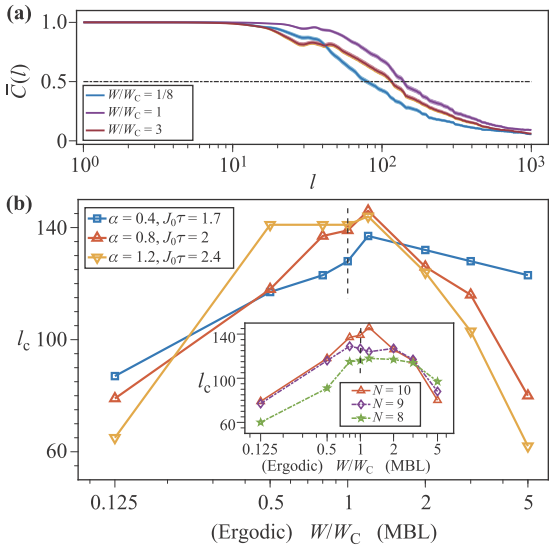

Fig. 5 The quantum reservoir learning performance on the Mackey–Glass task. The normalized covariance $\overline{C}$ characterizes the learning performance of this chaotic time sequence prediction task. **(a)** The dependence of $\overline{C}$ on the number of forward time steps (l) for the reservoir computing to predict. Here we set the interaction exponent $\alpha = 0.8$, the time duration $J_0\tau = 2$, the number of subintervals $V = 10$, and the qubit number $N = 10$. The results are calculated by averaging over 300 samples, with the standard deviations illustrated by the shaded error bands. Each learning task instance consists of 1000 time steps at the beginning discarded, the following 10000 time steps for training, and the last l time steps for prediction. The horizontal black "dash-dotted" line marks a threshold value of 0.5 (see the main text). A critical number of forward time steps l_c is defined as the point where $\overline{C}$ traverses the threshold value. **(b)** The critical number l_c as a function of disorder strength for different interaction exponents α and time duration τ. The inset shows the results with different qubit numbers $N = 8, 9, 10$, where we choose $\alpha = 0.8$, and $J_0\tau = 2$. The vertical black "dashed" lines in (b) indicate the MBL transition phase boundary. Here, the time durations τ for different exponent α are chosen to optimize the overall critical time step l_c.

quantum ergodic, and the MBL phases, respectively. This suggests the QRC has optimal learning power in between for learning tasks that requires both large memory capacity and sufficient nonlinearity. We thus analyze the MG task [31, 53] as such an example. This task is defined by [31]

$$F_{k+1} = \gamma F_k + \frac{\lambda F_{k-k_\Delta}}{1 + F_{k-k_\Delta}^{\beta}}, \tag{3}$$

with k_Δ a time delay. The dynamical system has a chaotic attractor with $k_\Delta > 16.8$, and here we choose $\gamma = 0.9$, $\beta = 10$, $\lambda = 0.2$, and $k_\Delta = 17$. We set $s_k = (F_k - F_{\min})/(F_{\max} - F_{\min})$, and $y_k^\star = s_{k+1}$ — the time sequences are shifted and rescaled to fit into the regime of $[0, 1]$ by introducing $F_{\max}$ and $F_{\min}$ in our numerical simulation. This learning task is to predict the chaotic time sequence, which is deterministic unlike the two tasks studied above. For the MG task, the output signals as measured from the reservoir (Fig. 1) are added with a slight amount of white noise in the range of $(-\sigma, \sigma)$ to improve robustness [20]. We choose $\sigma = 10^{-6}$ for the noise strength. In predicting the chaotic time sequence, i.e., for $k \in K_3$, s_k and y_k are decided through an iteration — y_k is obtained by giving the input s_k to the reservoir, and then y_{k+1} obtained by setting $s_{k+1} = y_k$. A piecewise linear threshold function is introduced here to enforce $y_k \in [0, 1]$ [54].

The QRC performance on this MG task strongly depends on the number of forward steps ($l = |K_3|$) to predict. The dependence of $\overline{C}$ on l is shown in Fig. 5(a). The QRC prediction for the chaotic time sequence works perfectly if the number of forward steps is small, producing $\overline{C} \approx 1$ for $l < 10$. It fails if l at request is too large. We remark here that the piecewise linear function is introduced only for numerical stability, and that the corresponding truncation is activated only when the reservoir computing starts to fail at large l. We then define a critical time step l_c, above which $\overline{C}$ drops down below a threshold (chosen to be 0.5 here). More discussions on the choice of the threshold value are provided in Appendix D. This critical time step quantifies the learning power of the quantum reservoir in predicting the chaotic time sequence. As shown in Fig. 5(b), as we vary the disorder strength, l_c develops a peak generically around the MBL localization transition point, as demonstrated for a broad range of $\alpha \in \{0.4, 0.8, 1.2\}$. This feature becomes more prominent for larger number of qubits. This finding implies the quantum reservoir has an optimal learning power near the edge of quantum ergodicity for complex learning tasks that require both memory and nonlinearity being sufficient.

7 Conclusion and outlook

We have investigated the learning power of a disordered quantum spin chain in both quantum ergodic and MBL phases. The MBL quantum reservoir is advantageous in holding long-term memory, for the presence of emergent local integrals of motion. The quantum ergodic phase provides a larger degree of nonlinearity, with a compromise on the memory holding. In dealing with the MG task that requires both memory capacity and nonlinearity, we find the learning performance develops a peak near the edge of the quantum ergodic phase, as analogous to the optimal computational power established for the classical reservoir computing at the edge of chaos. This leads to an important guiding principle of quantum reservoir engineering for complex reservoir computing tasks, that is to prepare the quantum system at the edge of quantum ergodicity. We expect our finding to hold in using other measures of quantum reservoir computing performance as well, for example with information processing capacity [55–57], for which the confirmation is worth future investigation.

Acknowledgements This work was supported by the National Program on Key Basic Research Project of China (Grant Nos. 2021YFA1400900 and 2017YFA0304204), the National Natural Science Foundation of China (Grant Nos. 11774067 and 11934002), Shanghai Municipal Science and Technology Major Project (Grant No. 2019SHZDZX01), Shanghai Science Foundation (Grant No. 19ZR1471500), and the Open Project of Shenzhen Institute of Quantum Science and Engineering (Grant No. SIQSE202002). X.Q. acknowledges support from the National Postdoctoral Program for Innovative Talents of China under Grant No. BX20190083.

Appendices

A Information encoding method

In this section, we show that the information encoding with the σ_x basis produces a much higher learning performance than the encoding with the σ_z basis, despite the local integrals of motion is mostly overlapped with σ_z operators. Intuitively, one would think the σ_z basis should be used for information encoding, since this basis possesses the localized degrees of freedom with no relaxation in the many-body localized (MBL) phase, and hence may lead to more memory capacity. However, we find that this naïve encoding does not give satisfactory learning performance. The reason is that the stored information with the encoding protocol would be washed away by the newly injected information that flows in. In order to resolve this problem, we encode the information in the σ_x basis. This allows the information to be stored collectively due to a logarithmically slow dephasing process present in the MBL phase [58]. Therefore, MBL provides sufficient memory capacity. The numerical results are shown in Fig. A1. Hereafter all the notations in the caption of the supplementary figures are the same as that in the main text. We find that information encoding with the σ_x basis indeed gives better learning performance for both the short-term memory (STM) and the parity check (PC) tasks. In contrast, the learning performance using information encoding with the σ_z basis is quite unsatisfactory.

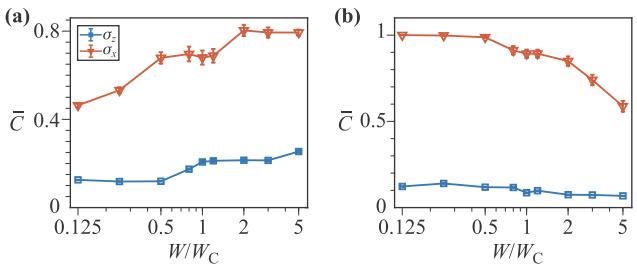

Fig. A1 Comparison of quantum reservoir learning performance between two different encoding protocols in σ_z and σ_x basis. The disorder potential is added to the σ_z basis. **(a)** shows the performance on the short-term memory task. **(b)** shows the parity check task. The performance of the reservoir computing is quantified by an averaged normalized covariance $\overline{C}$ (see the main text). Here, we set the qubit number $N = 10$, the number of subintervals $V = 10$, the time delay $k_\Delta = 16$ ($k_\Delta = 4$) for STM (PC) task, the time duration $J_0\tau = 0.3$ ($J_0\tau = 1$) for STM (PC) task, and the interaction exponent $\alpha = 0.4$. The results are averaged over 100 random samples, with the statistical error provided in the plot.

B The underlying mechanism for the quantum reservoir computing performance

In the main text, we have found that many-body localized (MBL) phases have memory capacities, whereas many-body ergodic phases possess nonlinear capacities. We point out that the former is due to an extensive number of quasilocal integrals of motion [26–29], and the latter is a result of the highly nonlocal correlations. In this section, we provide more results supporting these statements.

Here, to analyze the contribution of each qubit to the reservoir learning output, we perform two types of numerical tests, A and B, choosing a subset of qubit readout for producing reservoir learning output. For A, we choose the i-th qubit only and pass the corresponding observable to the linear regression model of the reservoir computing framework (see the main text). The corresponding results of the quantum reservoir at MBL and ergodic phases are shown in Figs. A2(a) and (b), respectively. For B we choose a subset of i-qubits (from 1 to i), and pass their

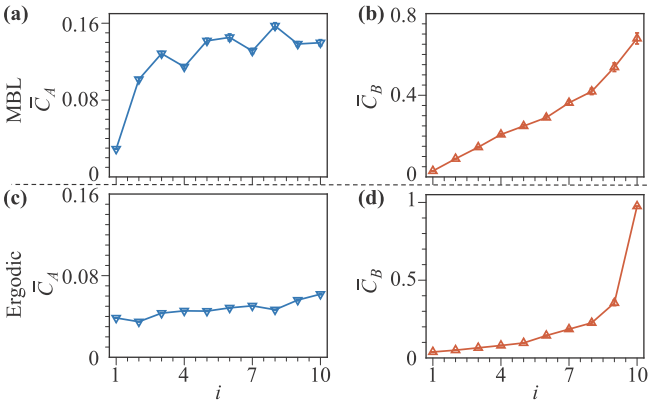

Fig. A2 The quantum reservoir learning performance on short-term memory tasks in the many-body localized phase, and parity check tasks in the ergodic phase for type A and B tests (see Sec. D). **(a)** shows the type A test for the short-term memory task with MBL reservoir. **(b)** The type A test for the parity check task with ergodic reservoir. **(c)** The type B test for short-term memory task with MBL reservoir. **(d)** The type B test for the parity check with ergodic reservoir. Here, we set the interaction exponent $\alpha = 0.4$, the disordering $W/W_C = 5$ ($W/W_C = 1/8$), the time duration $J_0\tau = 0.3$ ($J_0\tau = 10$), the time delay $k_\Delta = 16$ ($k_\Delta = 4$) for short-term memory tasks (parity check tasks), the number of subintervals $V = 10$, and the qubit number $N = 10$. The results are calculated by averaging over 100 samples.

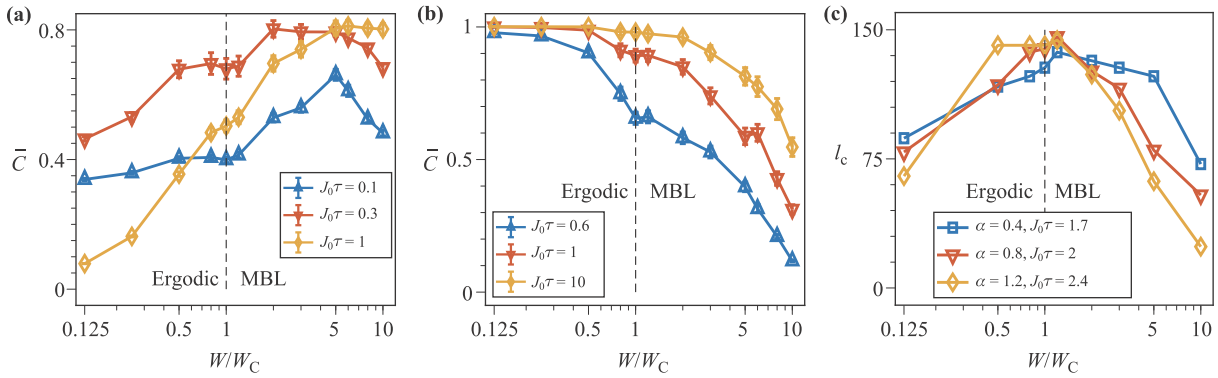

Fig. A3 The quantum reservoir learning performance on **(a)** short-term memory, **(b)** parity check tasks, and **(c)** Mackey–Glass task, which are the extensions of Fig. 2, Fig. 3, and Fig. 5(b) in the main text, respectively. Here, more numerical results in the deep MBL phase are provided, and the parameters in these three figures are chosen as same as that in the corresponding figures in the main text.

observables to the linear regression model. The corresponding results of the quantum reservoir at MBL and ergodic phases are shown in Figs. A2(c) and (d), respectively.

From the results in Fig. A2, it is evident that the learning behavior in the MBL and quantum ergodic phases are rather different. In the MBL phase, each qubit readout contributes to the eventual learning performance to a certain finite amount [Fig. A2(a)]. The exception is the first qubit, the reason is that the stored information in this qubit would be washed away by the newly injected information that flows in reservoir computing. In Fig. A2(b), we find the learning performance grows linearly with i, which implies the stored information in a MBL reservoir has an additive feature, revealing the weakly-entangled nature of the MBL wave function, a consequence of quasi local integrals of motion [47, 48]. The learning behavior is drastically different in the ergodic phase as shown in Figs. A2(c) and (d). The contribution of each qubit readout to the eventual learning performance is rather tiny [Fig. A2(c)]. As we increase i in Fig. A2(d), the learning performance remains quite low, and shows a sudden rise at when i reaches the total qubit number. This implies the information is processed in a global and collective manner in the ergodic phase. Since the mapping of the local input to the globally shared collective information necessarily involves a process of complex operator growth in dynamics, a quantum ergodic reservoir then naturally has more nonlinearity.

C Numerical results in the deep many-body localized phase

In this section, we provide more numerical results in the deep MBL phase, which are shown in Fig. A3. We find that for PC and Mackey–Glass (MG) task, the quantum reservoir learning performance decreases monotonously with the disordering in the MBL phase, which is in consistent with our previous analysis. Intuitively, one would expect that for the STM task, the quantum reservoir learning performance should increase monotonously with the disordering in the MBL phase. But this is not the case, as illustrated in Fig. A3(a). The reason is that in the very deep MBL phase, it is difficult for the input information propagating from the first qubit to the others, and the same time the information stored at the first qubit will be washed away by the newly injected information that flows in. We thus conclude the deep MBL phase is a bad choice for quantum reservoir computing for trivial reasons. Since we aim at constructing reservoir dynamics for an optimal quantum reservoir computing in this work, the deep MBL phase is not of our interest here.

D Results with varying capacity threshold for the Mackey–Glass task

In order to confirm our finding, namely the optimal quantum reservoir computing power near the MBL-to-ergodic phase transition, is robust, we present more results for the Mackey–Glass task with a different choice of the learning capacity threshold in this section. In the main paper, we choose a capacity threshold of 0.5 (see the main text). Here, we use a larger threshold of 0.7. The results are shown in Fig. A4. The dependence of capacity $\overline{C}$ on the time step l is shown in Fig. A4(a). The dashed line marks a threshold value of 0.7 and the dotted line represents the average time steps taken when calling the piecewise linear function for the first time. For the threshold value of 0.7, the critical time step l_c appears before the piecewise linear function is called for the first time. In this case, the piecewise linear function makes no contribution to the learning capacity. The corresponding results for l_c across the MBL-to-ergodic phase transition is shown in Fig. A4(b), where we still find an optimal quantum reservoir learning

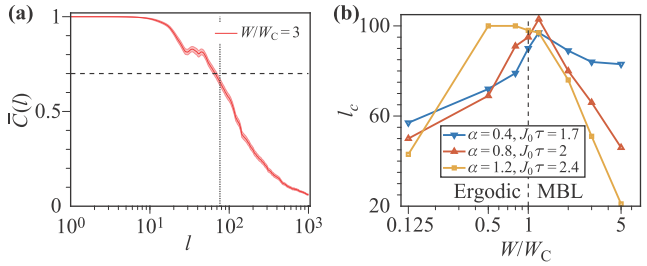

Fig. A4 The quantum reservoir learning performance on the Mackey–Glass task. **(a)** The dependence of $\overline{C}$ on the number of forward time steps (l) for the reservoir computing to predict. The dashed line indicates a threshold value of 0.7, while the dotted line represents the average time steps taken when calling the function for the first time. **(b)** The critical number l_c as a function of disorder strength for different interaction exponents α and time durations τ. The parameters in the figures are chosen as same as that in the corresponding figures in the main text.

power near the MBL-to-ergodic phase transition.

References

1. F. Arute, K. Arya, R. Babbush, D. Bacon, J. C. Bardin, et al., Quantum supremacy using a programmable superconducting processor, *Nature* 574(7779), 505 (2019)
2. H. S. Zhong, H. Wang, Y. H. Deng, M. C. Chen, L. C. Peng, Y. H. Luo, J. Qin, D. Wu, X. Ding, Y. Hu, P. Hu, X. Y. Yang, W. J. Zhang, H. Li, Y. Li, X. Jiang, L. Gan, G. Yang, L. You, Z. Wang, L. Li, N. L. Liu, C. Y. Lu, and J. W. Pan, Quantum computational advantage using photons, *Science* 370(6523), 1460 (2020)
3. J. Preskill, Quantum computing in the NISQ era and beyond, *Quantum* 2, 79 (2018)
4. I. H. Deutsch, Harnessing the power of the second quantum revolution, *PRX Quantum* 1(2), 020101 (2020)
5. E. Altman, K. R. Brown, G. Carleo, L. D. Carr, E. Demler, et al., Quantum simulators: Architectures and opportunities, *PRX Quantum* 2(1), 017003 (2021)
6. C. Gross and I. Bloch, Quantum simulations with ultracold atoms in optical lattices, *Science* 357(6355), 995 (2017)
7. F. Flamini, N. Spagnolo, and F. Sciarrino, Photonic quantum information processing: A review, *Rep. Prog. Phys.* 82(1), 016001 (2019)
8. J. Wang, F. Sciarrino, A. Laing, and M. G. Thompson, Integrated photonic quantum technologies, *Nat. Photonics* 14(5), 273 (2020)
9. M. Kjaergaard, M. E. Schwartz, J. Braumüller, P. Krantz, J. I. J. Wang, S. Gustavsson, and W. D. Oliver, Superconducting qubits: Current state of play, *Annu. Rev. Condens. Matter Phys.* 11(1), 369 (2020)
10. F. A. Zwanenburg, A. S. Dzurak, A. Morello, M. Y. Simmons, L. C. L. Hollenberg, G. Klimeck, S. Rogge, S. N. Coppersmith, and M. A. Eriksson, Silicon quantum electronics, *Rev. Mod. Phys.* 85(3), 961 (2013)
11. Y. Alexeev, D. Bacon, K. R. Brown, R. Calderbank, L. D. Carr, F. T. Chong, B. DeMarco, D. Englund, E. Farhi, B. Fefferman, A. V. Gorshkov, A. Houck, J. Kim, S. Kimmel, M. Lange, S. Lloyd, M. D. Lukin, D. Maslov, P. Maunz, C. Monroe, J. Preskill, M. Roetteler, M. J. Savage, and J. Thompson, Quantum computer systems for scientific discovery, *PRX Quantum* 2(1), 017001 (2021)
12. R. Mengoni, D. Ottaviani, and P. Iorio, Breaking RSA security with a low noise D-wave 2000Q quantum annealer: Computational times, limitations and prospects, arXiv: 2005.02268 (2020).
13. P. Hauke, H. G. Katzgraber, W. Lechner, H. Nishimori, and W. D. Oliver, Perspectives of quantum annealing: Methods and implementations, *Rep. Prog. Phys.* 83(5), 054401 (2020)
14. K. Nakajima, Physical reservoir computing — an introductory perspective, *Jpn. J. Appl. Phys.* 59(6), 060501 (2020)
15. N. H. Packard, Adaptation Toward the Edge of Chaos, in: Dynamic Patterns in Complex Systems, World Scientific, 1988, pp 293–301
16. C. G. Langton, Computation at the edge of chaos: Phase transitions and emergent computation, *Physica D* 42(1–3), 12 (1990)
17. N. Bertschinger and T. Natschläger, Real-time computation at the edge of chaos in recurrent neural networks, *Neural Comput.* 16(7), 1413 (2004)
18. R. Legenstein and W. Maass, Edge of chaos and prediction of computational performance for neural circuit models, *Neural Netw.* 20(3), 323 (2007)
19. M. Rafayelyan, J. Dong, Y. Tan, F. Krzakala, and S. Gigan, Large-scale optical reservoir computing for spatiotemporal chaotic systems prediction, *Phys. Rev. X* 10(4), 041037 (2020)
20. K. Fujii and K. Nakajima, Harnessing disordered-ensemble quantum dynamics for machine learning, *Phys. Rev. Appl.* 8(2), 024030 (2017)
21. S. Ghosh, A. Opala, M. Matuszewski, T. Paterek, and T. C. H. Liew, Quantum reservoir processing, *npj Quantum Inf.* 5, 35 (2019)
22. J. Chen, H. I. Nurdin, and N. Yamamoto, Temporal information processing on noisy quantum computers, *Phys. Rev. Appl.* 14(2), 024065 (2020)
23. S. Ghosh, A. Opala, M. Matuszewski, T. Paterek, and T. C. H. Liew, Reconstructing quantum states with quantum reservoir networks, *IEEE Trans. Neural Netw. Learn. Syst.* 32(7), 1 (2020)
24. J. Nokkala, R. Martínez-Peña, G. L. Giorgi, V. Parigi, M. C. Soriano, and R. Zambrini, Gaussian states of continuous-variable quantum systems provide universal and versatile reservoir computing, *Commun. Phys.* 4(1), 53 (2021)
25. K. Fujii and K. Nakajima, Quantum reservoir computing: A reservoir approach toward quantum machine learning on near-term quantum devices, arXiv: 2011.04890 (2020)
26. M. Serbyn, Z. Papić, and D. A. Abanin, Local conservation laws and the structure of the many-body localized states, *Phys. Rev. Lett.* 111(12), 127201 (2013)
27. D. A. Huse, R. Nandkishore, and V. Oganesyan, Phenomenology of fully many-body-localized systems, *Phys. Rev. B* 90(17), 174202 (2014)

28. V. Ros, M. Müller, and A. Scardicchio, Integrals of motion in the many-body localized phase, *Nucl. Phys. B* 891, 420 (2015)
29. A. Chandran, I. H. Kim, G. Vidal, and D. A. Abanin, Constructing local integrals of motion in the many-body localized phase, *Phys. Rev. B* 91(8), 085425 (2015)
30. D. A. Abanin, E. Altman, I. Bloch, and M. Serbyn, Many-body localization, thermalization, and entanglement, *Rev. Mod. Phys.* 91(2), 021001 (2019)
31. M. C. Mackey and L. Glass, Oscillation and chaos in physiological control systems, *Science* 197(4300), 287 (1977)
32. R. Martínez-Peña, G. L. Giorgi, J. Nokkala, M. C. Soriano, and R. Zambrini, Dynamical phase transitions in quantum reservoir computing, *Phys. Rev. Lett.* 127(10), 100502 (2021)
33. A. O. Maksymov and A. L. Burin, Many-body localization in spin chains with long-range transverse interactions: Scaling of critical disorder with system size, *Phys. Rev. B* 101(2), 024201 (2020)
34. L. M. K. Vandersypen and I. L. Chuang, NMR techniques for quantum control and computation, *Rev. Mod. Phys.* 76(4), 1037 (2005)
35. L. M. Duan and C. Monroe, Quantum networks with trapped ions, *Rev. Mod. Phys.* 82(2), 1209 (2010)
36. J. M. Pino, J. M. Dreiling, C. Figgatt, J. P. Gaebler, S. A. Moses, M. S. Allman, C. H. Baldwin, M. Foss-Feig, D. Hayes, K. Mayer, C. Ryan-Anderson, and B. Neyenhuis, Demonstration of the trapped-ion quantum CCD computer architecture, *Nature* 592(7853), 209 (2021)
37. A. Browaeys and T. Lahaye, Many-body physics with individually controlled Rydberg atoms, *Nat. Phys.* 16(2), 132 (2020)
38. D. W. Leung, I. L. Chuang, F. Yamaguchi, and Y. Yamamoto, Efficient implementation of coupled logic gates for quantum computation, *Phys. Rev. A* 61(4), 042310 (2000)
39. J. Li, R. Fan, H. Wang, B. Ye, B. Zeng, H. Zhai, X. Peng, and J. Du, Measuring out-of-time-order correlators on a nuclear magnetic resonance quantum simulator, *Phys. Rev. X* 7(3), 031011 (2017)
40. J. Smith, A. Lee, P. Richerme, B. Neyenhuis, P. W. Hess, P. Hauke, M. Heyl, D. A. Huse, and C. Monroe, Many-body localization in a quantum simulator with programmable random disorder, *Nat. Phys.* 12(10), 907 (2016)
41. J. Zhang, P. W. Hess, A. Kyprianidis, P. Becker, A. Lee, J. Smith, G. Pagano, I. D. Potirniche, A. C. Potter, A. Vishwanath, N. Y. Yao, and C. Monroe, Observation of a discrete time crystal, *Nature* 543(7644), 217 (2017)
42. X. Wu, X. Liang, Y. Tian, F. Yang, C. Chen, Y. C. Liu, M. K. Tey, and L. You, A concise review of Rydberg atom based quantum computation and quantum simulation, *Chin. Phys. B* 30(2), 020305 (2020)
43. M. Morgado and S. Whitlock, Quantum simulation and computing with Rydberg-interacting qubits, *AVS Quantum Science* 3(2), 023501 (2021)
44. X. Qiu, P. Zoller, and X. Li, Programmable quantum annealing architectures with Ising quantum wires, *PRX Quantum* 1(2), 020311 (2020)
45. D. A. Roberts, D. Stanford, and A. Streicher, Operator growth in the SYK model, *J. High Energy Phys.* 2018(6), 122 (2018)
46. X. Li, G. Zhu, M. Han, and X. Wang, Quantum information scrambling through a high-complexity operator mapping, *Phys. Rev. A* 100(3), 032309 (2019)
47. J. H. Bardarson, F. Pollmann, and J. E. Moore, Unbounded growth of entanglement in models of many-body localization, *Phys. Rev. Lett.* 109(1), 017202 (2012)
48. M. Serbyn, Z. Papić, and D. A. Abanin, Universal slow growth of entanglement in interacting strongly disordered systems, *Phys. Rev. Lett.* 110(26), 260601 (2013)
49. M. Serbyn, M. Knap, S. Gopalakrishnan, Z. Papić, N. Y. Yao, C. R. Laumann, D. A. Abanin, M. D. Lukin, and E. A. Demler, Interferometric probes of many-body localization, *Phys. Rev. Lett.* 113(14), 147204 (2014)
50. A. Larkin and Y. N. Ovchinnikov, Quasiclassical method in the theory of superconductivity, *Sov. Phys. JETP* 28, 1200 (1969)
51. S. H. Shenker and D. Stanford, Black holes and the butterfly effect, *J. High Energy Phys.* 2014(3), 67 (2014)
52. J. Maldacena, S. H. Shenker, and D. Stanford, A bound on chaos, *J. High Energy Phys.* 2016(8), 106 (2016)
53. H. Jaeger and H. Haas, Harnessing nonlinearity: Predicting chaotic systems and saving energy in wireless communication, *Science* 304(5667), 78 (2004)
54. K. Srinivasan, I. Raja Mohamed, K. Murali, M. Lakshmanan, and S. Sinha, Design of time delayed chaotic circuit with threshold controller, *Int. J. Bifurcat. Chaos* 21(3), 725 (2011)
55. J. Dambre, D. Verstraeten, B. Schrauwen, and S. Massar, Information processing capacity of dynamical systems, *Sci. Rep.* 2(1), 514 (2012)
56. R. Martínez-Peña, J. Nokkala, G. L. Giorgi, R. Zambrini, and M. C. Soriano, Information processing capacity of spin-based quantum reservoir computing systems, *Cognit. Comput.* (2020)
57. J. Nokkala, R. Martínez-Peña, G. L. Giorgi, V. Parigi, M. C. Soriano, and R. Zambrini, Gaussian states of continuous-variable quantum systems provide universal and versatile reservoir computing, *Commun. Phys.* 4(1), 53 (2021)
58. J. H. Bardarson, F. Pollmann, and J. E. Moore, Unbounded growth of entanglement in models of many-body localization, *Phys. Rev. Lett.* 109(1), 017202 (2012)